Quarter-filled supersolid and solid phases in the extended Bose–Hubbard model

2010 J. Phys.: Condens. Matter 22 185601

(http://iopscience.iop.org/0953-8984/22/18/185601)

IOP Publishing Journal of Physics: Condensed Matter

J. Phys.: Condens. Matter **22** (2010) 185601 (7pp) doi:10.1088/0953-8984/22/18/185601

Quarter-filled supersolid and solid phases in the extended Bose–Hubbard model

Kwai-Kong Ng, Y C Chen and Y C Tzeng[1]

Department of Physics, Tunghai University, Taichung 40704, Taiwan

Received 12 January 2010, in final form 29 March 2010
Published 20 April 2010
Online at stacks.iop.org/JPhysCM/22/185601

Abstract

We numerically study the ground state phase diagram of the two-dimensional hard-core Bose–Hubbard model with nearest-(V_1) and next-nearest-neighbour (V_2) repulsions. In particular, we focus on the quarter-filled phases where one supersolid and two solid phases are observed. Using both canonical and grand canonical quantum Monte Carlo (QMC) methods and a mean-field calculation, we provide evidence for the existence of a *commensurate* supersolid. Despite the two possible diagonal long-range orderings for the solid phase, only one kind of supersolid phase is found to be energetically stable. The competition between the two solid phases manifests itself as a first-order phase transition around $2V_2 \sim V_1$. The change of order parameters as a function of the chemical potential is also presented.

(Some figures in this article are in colour only in the electronic version)

The Bose–Hubbard model has recently attracted a lot of attention for the possibility of observing the supersolid phase [1] either in optical lattices [2] or in magnetic systems [3]. The simultaneous breaking of both translational and $U(1)$ gauge symmetry is a delicate state of matter so that only recently has experimental evidence of a possible supersolid phase been provided by the measurement of the non-classical rotational inertia (NCRI) [4] in rotating solid ^{4}He [5]. However, the observed NCRI may be attributed to the superflow between microcrystal interfaces and the issue is still largely controversial [6]. Thanks to technological advances in trapping atoms or even molecules at very low temperature in optical lattices, it provides an ideal testing ground for the search for the supersolid phase. The Hubbard model of hard-core bosons in a frustrated triangular lattice [7] and soft-core bosons [8] in a square lattice are among the possible candidates. Besides the optical lattice experiments, various magnetic systems have been suggested [3] to be candidates for the realization of a spin supersolid in some carefully chosen parameter regime. In the case of spin $S = \frac{1}{2}$, where the system is equivalent to the hard-core Bose–Hubbard model, the spin supersolid represents the state of spatial modulation of the in-plane spin projection.

The hard-core Bose–Hubbard model with only nearest-neighbour (nn) interactions on a square lattice has ground states of superfluid ordering and checkerboard solid ordering.

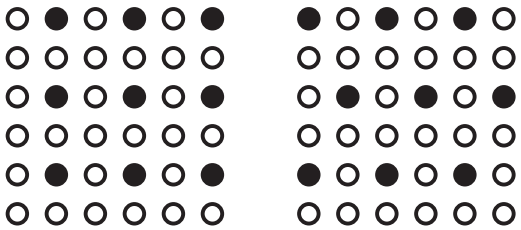

(a) Solid A (b) Solid B

Figure 1. Classical lattice structures of star solid (a) A and (b) B phases.

On the other hand, a sufficiently large next-nearest-neighbour (nnn) interaction leads to the checkerboard ordering being replaced by a striped ordering which can coexist with a superfluid to form a striped supersolid around half-filling [9]. Recently we revisited the model [10] and found a new solid phase with 'star' ordering (figure 1(a)) at quarter-filling. Interestingly, this star solid (A phase) ordering can also coexist with the superfluid ordering to form a star supersolid phase at and around quarter-filling. It has also been suggested [11] that another solid (B phase) order can be stabilized when $2V_2 > V_1$. However, whether the supersolid ground state with this solid ordering is stable is unclear and the complete ground state phase diagram including the B phase solid is still unavailable. These are the questions we attempt to address in this work. We also discuss the possibility of the existence of a commensurate

[1] Present address: Department of Physics, National Tsing Hua University, Hsinchu 30013, Taiwan.

supersolid, in which the particle number is commensurate with the solid structure, in the context of a vacancy supersolid. We will show in this paper that the quarter-filled star supersolid is commensurate but agrees with the notion of a vacancy supersolid.

Specifically, we study the extended Bose–Hubbard model on a 2D square lattice with the Hamiltonian

$$H_b = -t\sum_{i,j}^{nn}(b_i^\dagger b_j + b_i b_j^\dagger) + V_1\sum_{i,j}^{nn} n_i n_j + V_2\sum_{i,j}^{nnn} n_i n_j - \mu\sum_i n_i \quad (1)$$

where $b(b^\dagger)$ is the boson destruction (creation) operator and $\sum^{nn}(\sum^{nnn})$ sums over the (next-) nearest-neighbouring sites. For convenience we fix the energy scale by setting $t = 1$ throughout this paper. By taking the transformation $b^\dagger \rightarrow S^\dagger$ and $n \rightarrow S^z + \frac{1}{2}$, this Hamiltonian can be mapped to a spin XXZ model with nn and nnn exchange couplings under a magnetic field $h = \mu - \frac{z}{2}(V_1 + V_2)$ (z is the coordination number). At half-filling, the ground state of the Hamiltonian H_b is a checkerboard solid (characterized by wavevector $\mathbf{Q} = (\pi, \pi)$) for strong nn coupling V_1, or a striped solid (characterized by wavevector $\mathbf{Q} = (\pi, 0)$ or $(0, \pi)$) for strong nnn coupling V_2 [9]. For $V_1 \sim 2V_2$, quantum frustration destabilizes both solid orders and leads to a uniform superfluid phase. No supersolid phase is found at half-filling. Away from half-filling, however, a striped supersolid is observed for dominating nnn interaction $2V_2 > V_1$, while the checkerboard supersolid phase is still unstable against phase separation for large nn interaction $V_1 > 2V_2$. It has been argued that the motion of domain walls reduces the ground state energy so that the checkerboard supersolid is energetically unstable [8].

Further away from half-filling, new types of solids in the vicinity of quarter-filling, as well as three-quarter-filling, have been found very recently [10–12] as mentioned above. The A phase quarter-filled solid (see figure 1) has a finite structure factor $S(\mathbf{Q}) = \sum_{ij}\langle n_i n_j e^{i\mathbf{Q}\mathbf{r}_{ij}}\rangle/N^2$ at wavevectors $\mathbf{Q}_0 = (\pi, \pi)$, $(\pi, 0)$ and $(0, \pi)$, which implies a star-like occupation pattern. Moreover, doping the star solid with extra bosons yields a star supersolid via a second-order phase transition. The formation of domain walls is no longer energetically favourable and hence the star supersolid is stable upon doping instead of phase separation. More interestingly, this star supersolid persists even at exact quarter-filling for a wide range of parameters V_1 and V_2 (see figure 8). This result seems to contradict a recent proof [15] that the necessary condition for supersolidity is to have zero-point vacancies or defects and that no commensurate supersolid is possible. Reference [11, 12] claims they do not observe a quarter-filled star supersolid in their QMC data. Unfortunately, no data on the structure factor and superfluidity are presented in the right V_1, V_2 parameter regime where we observed the quarter-filled supersolid. One natural question that arises about the discrepancy is whether a canonical approach, used in [12] where particle number is fixed, leads to different results. In order to clarify the issue, we provide further evidence using a Green's function Monte Carlo (GFMC) method to support the existence of a quarter-filled supersolid.

1. Stochastic series expansion

In order to clarify the issue of the presence of the SS phase at $n = 0.25$, we numerically study the model with both the grand canonical and canonical approaches. The grand canonical calculation is carried out using the standard stochastic series expansion (SSE) Monte Carlo method implemented with a directed loop algorithm [13]. While SSE works on the grand canonical ensemble, in order to fix the density n we scan the chemical potential μ to find an average density $\langle n\rangle = 0.25$ with an uncertainty less than 0.01. It turns out, as shown below, that this method generates the same result as the GFMC. In SSE, the superfluidity, given by $\rho_{x(y)} = \langle W^2_{x(y)}\rangle/4\beta t$, is computed by measuring the winding number fluctuation as usual.

2. Green's function Monte Carlo

The GFMC starts with a Jastrow variational wavefunction, which is defined by applying the density Jastrow factor to a state with all the bosons condensed into the $q = 0$ state:

$$|\Psi_J\rangle = \exp\left\{-\tfrac{1}{2}\sum_{ij} v_{i,j} n_i n_j\right\}|\Phi_0\rangle, \quad (2)$$

where $|\Phi_0\rangle = (\sum_i b_i^\dagger)^N|0\rangle$ is the non-interacting boson ground state with N particles and $v_{i,j}$ are parameters that can be optimized to minimize the variational energy [14]. In order to take the hard-core constraint into account, configurations with more than one boson on a single site are projected out from (2). The wavefunction $|\Psi_J\rangle$ in (2) was shown to be able to turn a non-interacting bosonic state into a Mott insulator if a long-range Jastrow factor is included. In our recent work, we have also shown that the supersolid and solid phases can also be described in the same wavefunction. However, the number of variational parameters in $v_{i,j}$ grows exponentially with the lattice size which costs a lot of computation time for an optimized wavefunction. Instead of including parameters of all ranges, we use a Gutzwiller projection factor $\exp\left\{\sum_{i\in A} g n_i\right\}$ to enhance the diagonal order. Here g is a variational parameter which controls the diagonal order specified by the sublattice A. Obviously, this factor can stabilize the solid and gives a reasonably good trial energy when V_1 and V_2 are large. We found that a low variational energy can be acquired for the A-type supersolid and solid without the projection factor. On the other hand, a relatively stable wavefunction is found by including the projection factor for the B-type solid.

In order to investigate the exact ground state properties, the Green's function Monte Carlo method is employed to improve the variational results. In this work, we choose the multi-walker stochastic reconfiguration method to prevent the simulation from blow-up or dead-ends in the large power limit. To benchmark our method we compare our GFMC data (points) with the exact results (lines) without using Monte Carlo for a 6×6 lattice in figure 2. We can see that the GFMC results are consistent with the exact ones. The underestimation of the diagonal order in the variational wavefunction is corrected as the number of iterations increases. We have verified that the same ground state properties can also

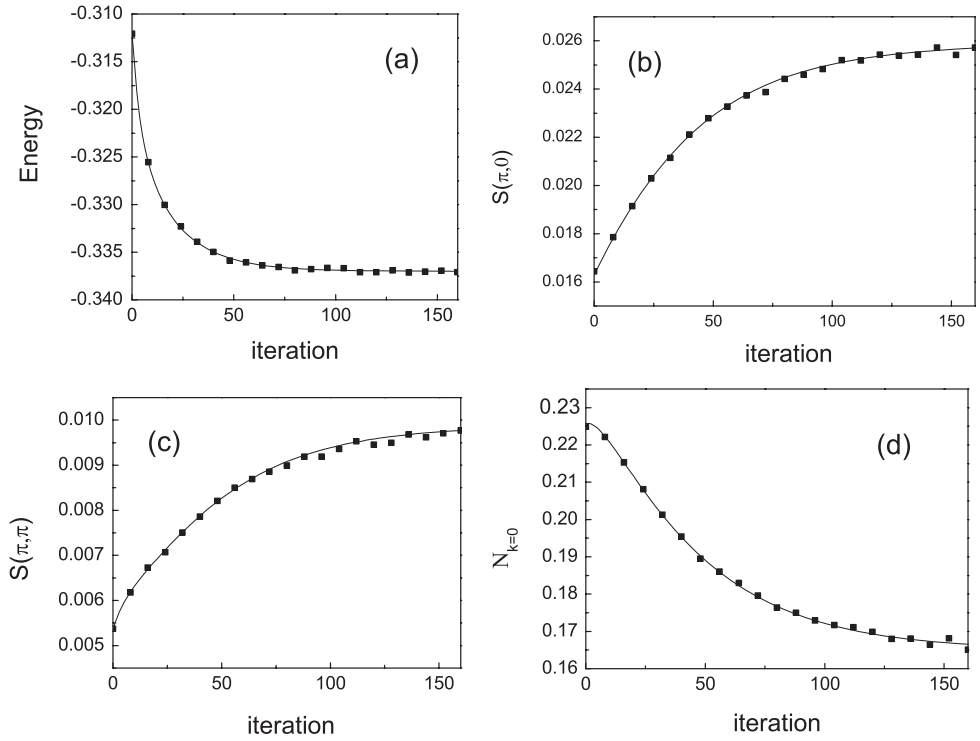

Figure 2. (a) Ground state energy, structure factor (b) $S(\pi, 0)$, (c) $S(\pi, \pi)$ and (d) condensate density $N_{k=0}$ obtained by GFMC of a 6×6 lattice ($V_1 = 2$, $V_2 = 4.5$), at quarter-filling $n = 0.25$ as a function of iteration The guiding function is the same as trial wavefunction with $v_{1,0} = 0.9$, $v_{1,1} = 0.83$. 4000 walkers are used in the GFMC calculation.

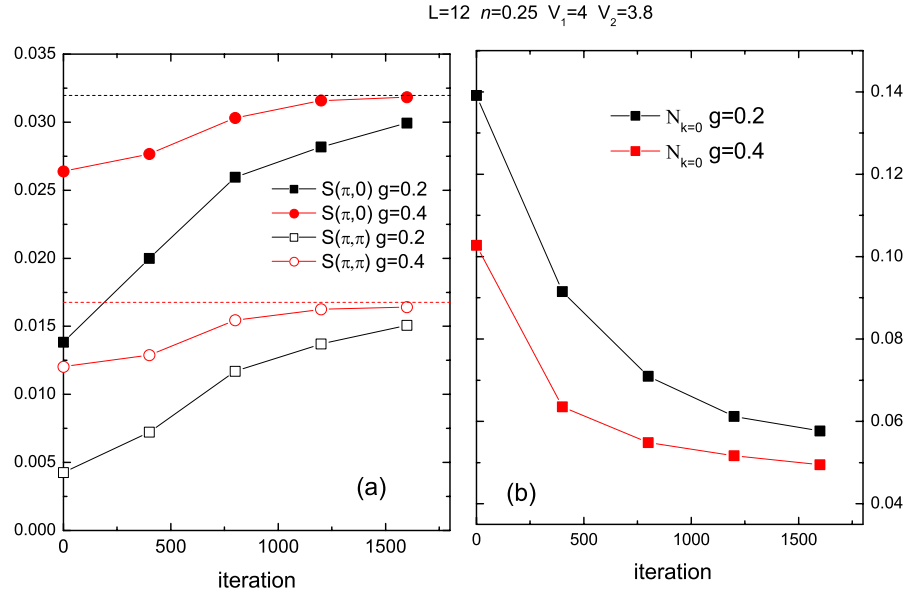

Figure 3. (a) Structure factors $S(\pi, 0)$ and $S(\pi, \pi)$ and (b) condensate density $N_{k=0}$ obtained by GFMC for lattice 12×12 ($V_1 = 4$, $V_2 = 3.8$) at $n = 0.25$ as a function of iteration number. Two variation parameters $g = 0.2, 0.4$ are shown. Dashed lines are results obtained from SSE for comparison.

be obtained by using the wavefunction with diagonal order ($g \neq 0$).

Now we present the GFMC results for a larger lattice. In figure 3 we show the structure factors and condensate $N_{k=0} = b^{\dagger}_{k=0} b_{k=0}$ as a function of iteration number. The trial wavefunction with A-type diagonal order is used as the trial wavefunction. In order to check that the ground state can be reached, regardless of the choice for g, we present results of $g = 0.2$ and 0.4. The wavefunction is optimized for all parameters before GFMC is applied. The corresponding data obtained by SSE (dashed lines) are also shown for comparison. As we can see, although the optimized wavefunction overestimated the structure factor and underestimated the condensate density, consistent results

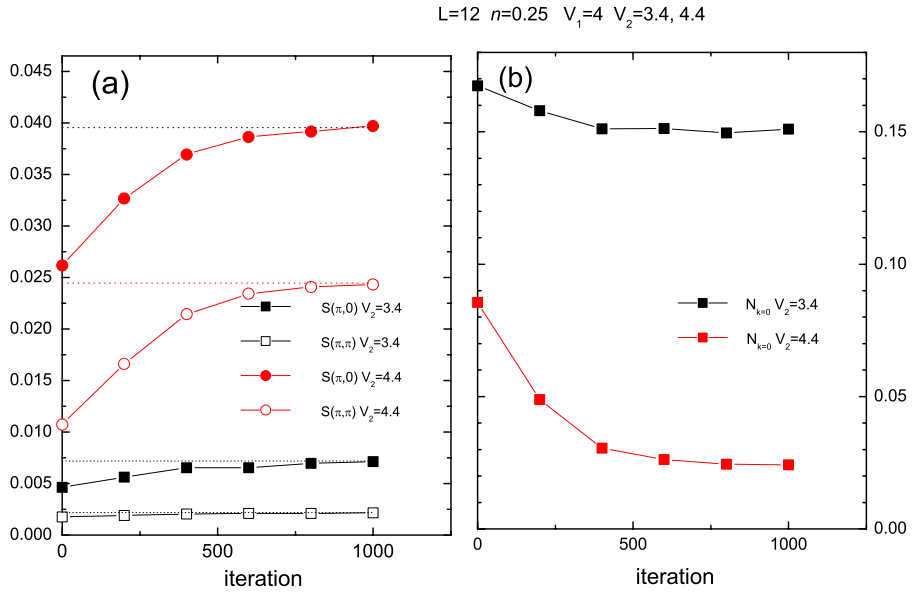

Figure 4. The same as figure 3 but here $V_2 = 3.4$ and 4.4.

with SSE are obtained as the number of iterations increases. Figure 4 shows similar calculations for $V_2 = 3.4$ and 4.4, corresponding to superfluid and A-type solid phases, respectively. The data clearly show the convergence of the GFMC approach and are consistent with the SSE results.

3. Mean-field theory

To further investigate the effect of quantum fluctuations on the model, we also obtain the ground state phase diagram using a simple mean-field approach. A mean-field wavefunction

$$|\Psi\rangle_{\mathrm{MF}} = \prod_{i,\alpha}(u_i|1\rangle_{i,\alpha} + v_i|0\rangle_{i,\alpha}) \tag{3}$$

is given to represent the superfluid, star solid and star supersolid phases. Here α denotes the index of a 2×2 unit cell while $i = 1, 2, 3, 4$ is the sublattice index inside the cell. $|1\rangle_{i,\alpha}$ ($|0\rangle_{i,\alpha}$) is the occupied (empty) Fock state at the ith site of the unit cell α while $u_i(v_i)$ is the corresponding variational parameter. The energy of $|\Psi\rangle_{\mathrm{MF}}$ is then minimized to obtain the ground state wavefunction. This MF wavefunction successfully predicts the existence of a quarter-filled star supersolid as well as the superfluid and star solid as shown in the inset of figure 8.

4. Quarter-filled supersolid

Figure 5 shows the result of SSE and GFMC at $V_1 = 4$ and 8 for small lattice size. The agreement between both approaches is clear and verifies that our attempt to fix the boson density n to 0.25 in the grand canonical SSE does not lead to any measurable discrepancy of the physical quantities we are interested in with the canonical GFMC. The fact that the condensate density $N_{k=0}$ is found to be larger than the superfluid density ρ_x in some of the data in figure 5 originates solely from the small size ($L = 12$) we used in this

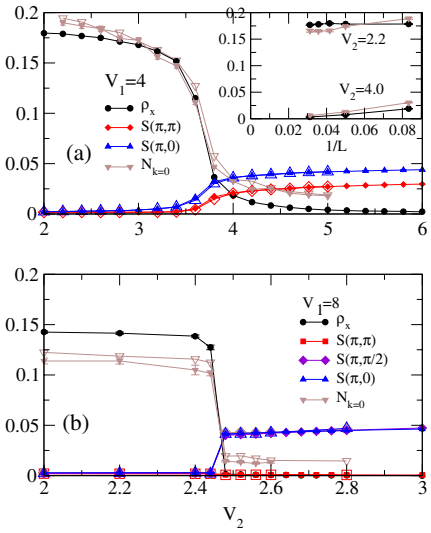

Figure 5. Comparison of data obtained from the SSE (filled symbols) and GFMC (open symbols) for lattice size $L = 12$. We show in the inset the finite size behaviour of the QMC data of ρ_x and $N_{k=0}$ for $V_2 = 2.2, 4.0$ and $V_1 = 2.0$. Temperature used in the SSE is $T/t = 0.02$.

comparison. In the inset, we plot the QMC data of ρ_x and $N_{k=0}$ as a function of $1/L$ to show the finite size scaling behaviour at two typical points of $V_2 = 2.2$ and 4.0, respectively, for $V_1 = 2.0$. In the superfluid phase with $V_2 = 2.2$, $N_{k=0}$ drops below ρ_x for $L \geqslant 20$ as both quantities scale similarly and converge to finite values when $L \geqslant 24$. For the case of $V_2 = 4.0$, both ρ_x and $N_{k=0}$ converge to zero as $L \to \infty$, as expected in the solid phase. The coexistence of superfluid order and star crystal structure for $3.5 \lesssim V_2 \lesssim 4.0$ in figure 5(a) clearly signals the supersolid phase at quarter-filling. The uniform superfluid develops spatial modulation, i.e. becomes a supersolid, continuously as V_2 increases and gradually loses its superfluidity at the same time until it eventually becomes a star solid. To demonstrate that the supersolid ground state

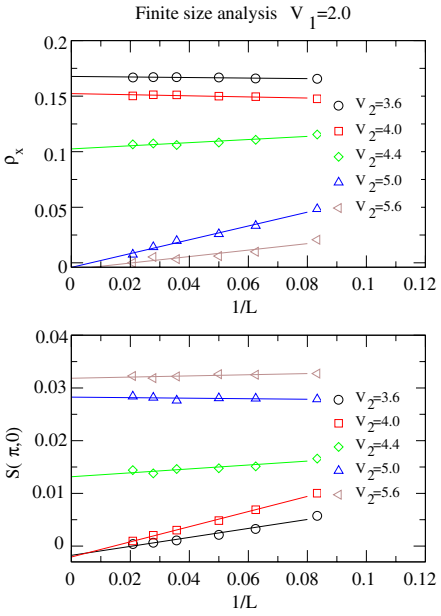

Figure 6. Finite size analysis of the order parameters ρ_x and $S(\pi, 0)$ from SSE for $V_1 = 2.0$.

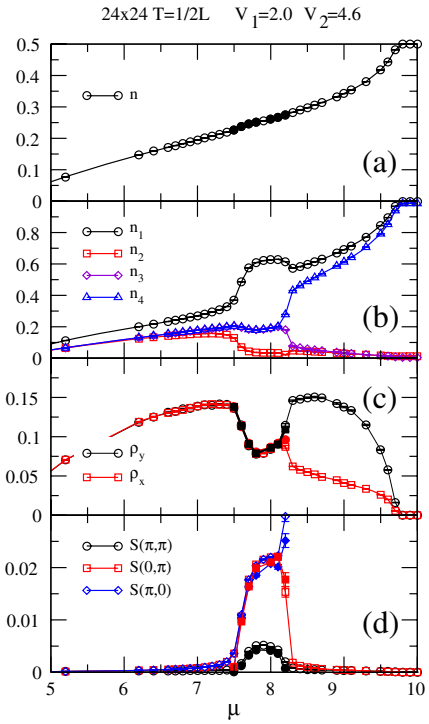

Figure 7. SSE result of (a) average density n, (b) sublattice densities, (c) superfluidity and (d) structure factors as a function of chemical potential μ for $V_1 = 2.0$ and $V_2 = 4.6$. Open (filled) symbols denote the result for lattice size 24×24 (48×48).

survives at larger lattice size and at the thermodynamic limit, a finite size analysis is carried out in figure 6 for $V_1 = 2$. $S(\pi, 0)$ scales to zero in the superfluid phase whereas ρ_x scales to zero in the solid phase. It is only in the supersolid phase ($V_2 = 4.4$ in figure 6) that both $S(\pi, 0)$ and ρ_x scale to finite values. It is remarkable that simple MF theory also correctly predicts the existence of a quarter-filled SS and quantum fluctuation does not destroy the long-range order in the SS phase, in contrast to the case of a Kagomé lattice [16]. Except that the solid A and B phase are indistinguishable in the MF level, MF theory successfully reproduces all phases at quarter-filling as shown in the inset of figure 8.

At first glance, the existence of a supersolid at *commensurate* density contradicts the notion of a vacancy supersolid. Prokof'ev and Svistunov [15] have proved that superfluidity has zero probability of occurring in commensurate solids in nature, or in other words, the necessary condition for the supersolidity is the presence of vacancies or defects. This is due to the asymmetry between vacancies and interstitials. However, this result, as admitted in their paper, does not apply to systems with explicitly broken translation symmetry, such as in lattice models where commensurability is enhanced by hand. In our system, the commensurability of the quarter-filled supersolid can always be ensured by adjusting the chemical potential provided there is no phase separation. Vacancies and interstitials (this means bosons at the sublattice sites) that arise from quantum fluctuations do not form bound pairs and are free to move away from each other and this, therefore, leads to superflow. The interstitial-vacancy symmetry is generally absent in nature but is preserved in this case by the external potential that fixes bosons only at the lattice points. Based on the measured structure factors $S(\pi, \pi)$, $S(\pi, 0)$ and $S(0, \pi)$ and boson density n, one can easily deduce the boson densities on each sublattice. Figure 7 shows that bosons are not localized at only one sublattice but have finite occupation in all four sublattices. The data indicate that there are more than 30% of vacancies in the quarter-filled supersolid, which is consistent with the picture of a vacancy supersolid.

To gain more insight of the quarter-filled supersolid phase, we plot in figure 7 the order parameters as functions of the chemical potential μ. Starting from small density, the ground state is an uniform superfluid in which all sublattice densities are equal. While increasing μ until quarter-filled, the system undergoes a second-order phase transition to a star SS. Note that, although there is a small dip of superfluidity in the SS state, it does not reduce to zero even at $n = 0.25$. There is no indication that $n = 0.25$ is a special density that acquires particular treatment like the canonical calculation. Furthermore, no noticeable change is observed when doubling the lattice size to 48×48 (filled symbols in figure 7). Doping more bosons will destabilize the star SS phase because of the nnn repulsion that leads to a striped SS via a discontinuous phase transition between the two different broken translation symmetries. Striped SS is also observable at $n = 0.25$ when V_1 is small enough. On the other hand, while there are two kinds of star solid (A and B phase), a natural question is whether SS of both kinds exist at or away from quarter-filled. We will address this issue in section 5.

5. Supersolid A and B phase

It is interesting to note that, at quarter-filling, the classical ground state of the frustrated Hamiltonian H is highly

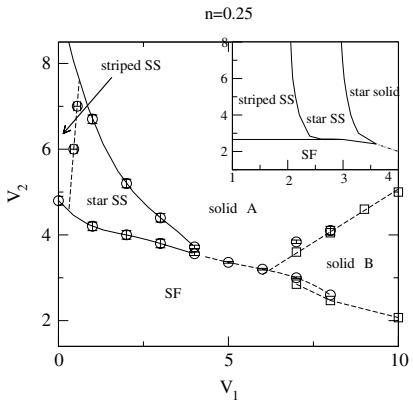

Figure 8. Ground state phase diagram of H_b for $n = 0.25$. The lines are guides to the eyes. Solid (dotted) lines represent second (first)-order phase transition boundaries. Black circles (squares) denote the data obtained from the SSE (GFMC) for $L = 28$ ($L = 16$). The inset shows the MF result. It is noted that star solid A and B phases cannot be distinguished in the MF level. There is a first-order phase transition from the star SS to striped SS phase for small V_1. We refer to [10] for detailed discussions of the striped SS.

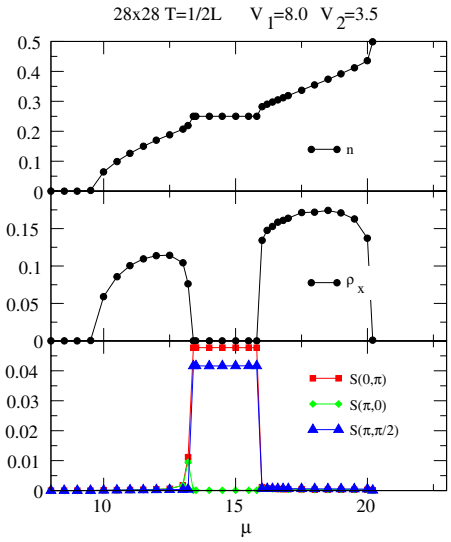

Figure 9. SSE results for $V_1 = 8.0$ and $V_2 = 3.5$. The ground state at $n = 0.25$ is a B phase solid. Doping away from $n = 0.25$ leads to a first-order phase transition to the SF phase. No B phase supersolid is found.

degenerate. Translating any lines of bosons in figure 1(a) by one lattice constant of the solid A phase along, say, the x direction will create a domain wall with no energy cost. Translating alternate lines of bosons generates a B phase solid. An enormous number of ways to create domain walls implies that the classical ground state has macroscopic degeneracy. This degeneracy, however, is lifted by quantum fluctuation that yields a ground state of A phase if $V_1 < 2V_2$ or B phase otherwise. This is another typical example of the order by disorder phenomenon [7]. As discussed in previous sections, it leads to a star SS A phase in a wide parameter range, similar to the scenario of the half-filling SS in the frustrated triangular lattice [7]. On the other hand, the existence of the

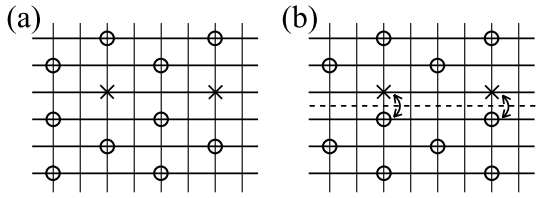

Figure 10. Hole doping on the quarter-filled solid B phase. (a) A single hole. (b) A line of holes forms a domain wall. (c) Shifting the bosons on one side has slightly (to the fourth order) larger energy gain. (d) Hopping of bosons along the domain wall leads to a kinetic energy gain larger than that of an isolated hole.

star SS B phase has not been clarified. Here we complete the phase diagram for larger V_1 where the solid B phase can be stabilized at quarter-filling. Figure 8 shows that, for $V_1 > 6$, when increasing from a small nnn interaction V_2, the SF phase changes to the solid B phase via a first-order phase transition without passing an intermediate SS B phase. The star solid A phase emerges when further increasing V_2 until $2V_2 \gtrsim V_1$. Furthermore we do not observe any SS B phase away from $n = 0.25$ as shown in figure 9 at a representative $V_1 = 8.0$ and $V_2 = 3.5$. Instead there is a first-order phase transition from the gapped solid B phase to a uniform SF phase which implies that the SS of B phase symmetry is unstable toward phase separation. This can be understood by the simple argument of domain formation as discussed in the case of hard-core checkerboard SS [8]. An extra hole in the quarter-filled solid phase B costs no potential energy but an increase in chemical potential μ (see figure 10(a)). The kinetic energy gain is $-2t^2/V_1 - 2t^2/V_2$ per hole. However, lining up the holes forms a domain wall in which hopping of bosons along the wall leads to a kinetic energy gain of $-2t$ (figure 10(d)). Therefore doping extra holes into the quarter-filled solid B phase leads to phase separation instead of a uniform SS phase. A similar argument applies for boson doping and hence no SS B phase is found to be stable.

6. Summary

We have presented a comprehensive numerical study on the extended hard-core Hubbard model, in particular, on the SS phases at the quarter-filled density. Based on results of the SSE, GFMC and MF calculations, we provide convincing evidence for the existence of the star SS A phase at exactly $n = 0.25$, in contrast to our previous study. We clearly show that the SS A phase found at $n = 0.25$ is consistent with the notion of a vacancy SS. The star SS phase is a consequence of the order by disorder phenomenon by which the ground state degeneracy is lifted. Furthermore, the physical natures of the solid A and B phases are also studied. Although classically degenerate, these two states compete with each other through quantum fluctuations and the final stability depends on the competition between nn (V_1) and nnn (V_2) interactions. We present a complete phase diagram including also the solid B phase. The SS B phase, on the other hand, is found to be unstable toward phase separation due to the kinetic energy gain of domain formation.

Acknowledgments

We are grateful to M F Yang for stimulating discussions. This work was supported by the NSC (R.O.C.), grant nos. NSC 97-2112-M-029-003-MY3 and NSC 96-2112-M029-003-MY3.

References

[1] Penrose O and Onsager L 1956 *Phys. Rev.* **104** 576
[2] Jaksch D, Bruder C, Cirac J I, Gardiner C W and Zoller P 1998 *Phys. Rev. Lett.* **81** 3108
Greiner M, Mandel O, Esslinger T, Hänsch T W and Bloch T 2002 *Nature* **415** 39
[3] Ng K K and Lee T K 2006 *Phys. Rev. Lett.* **97** 127204
Sengupta P and Batista C D 2007 *Phys. Rev. Lett.* **98** 227201
[4] Andreev A F and Lifshitz I M 1969 *Sov. Phys.—JETP* **29** 1107
Chester G V 1970 *Phys. Rev.* A **2** 256
Leggett A J 1970 *Phys. Rev. Lett.* **25** 1543
[5] Kim E and Chan M H W 2004 *Nature* **427** 225
Kim E and Chan M H W 2004 *Science* **305** 1941
[6] Burovski E, Kozik E, Kuklov A, Prokof'ev N and Svistunov B 2005 *Phys. Rev. Lett.* **94** 165301
Rittner A S C and Reppy J D 2006 *Phys. Rev. Lett.* **97** 165301
[7] Wessel S and Troyer M 2005 *Phys. Rev. Lett.* **95** 127205
Heidarian D and Damle K 2005 *Phys. Rev. Lett.* **95** 127206
Melko R *et al* 2005 *Phys. Rev. Lett.* **95** 127207
[8] Sengupta P, Pryadko L P, Alet F, Troyer M and Schmid G 2005 *Phys. Rev. Lett.* **94** 207202
[9] Batrouni G G and Scalettar R T 2000 *Phys. Rev. Lett.* **84** 1599
Hebert F *et al* 2001 *Phys. Rev.* B **65** 014513
[10] Ng K K and Chen Y C 2008 *Phys. Rev.* B **77** 052506
[11] Dang L, Boninsegni M and Pollet L 2008 *Phys. Rev.* B **78** 132512
[12] Chen Y C, Melko R G, Wessel S and Kao Y J 2008 *Phys. Rev.* B **77** 014524
[13] Sandvik A W 1999 *Phys. Rev.* B **59** R14157
Sandvik A W 1997 *Phys. Rev.* B **56** 11678
Syluåsen O F and Sandvik A W 2002 *Phys. Rev.* E **66** 046701
[14] Capello M, Becca F, Fabrizio M and Sorella S 2007 *Phys. Rev. Lett.* **99** 056402
Sorella S 2005 *Phys. Rev.* B **71** 241103(R)
[15] Prokof'ev N and Svistunov B 2005 *Phys. Rev. Lett.* **94** 155302
[16] Isakov S V, Wessel S, Melko R G, Sengupta K and Kim Y B 2006 *Phys. Rev. Lett.* **97** 147202